Early Warning of Stability Loss via Predictability and Local Linearization in Nonlinear Dynamical Systems

Mohamed Oussama Najar

1 Introduction

Many natural and engineered systems undergo abrupt transitions between qualitatively distinct dynamical regimes. Anticipating loss of stability *prior* to such transitions is a central challenge in monitoring, forecasting, and control. Classical early warning indicators—such as increasing variance or autocorrelation associated with critical slowing down—can provide useful signals, but often rely on assumptions of stationarity, linearization near equilibrium, or stochastic forcing that may not hold in nonlinear, deterministic, or externally forced systems [5].

Empirical Dynamic Modeling (EDM) offers an equation-free framework for analyzing nonlinear dynamics directly from time series data. Rather than relying solely on moment-based statistics, EDM reconstructs state-space geometry from observations and evaluates predictability and local linear structure as emergent properties of the observed dynamics [1, 3, 4]. Changes in forecast skill or local linearization can therefore be interpreted as signatures of evolving stability and state dependence, even when governing equations are unknown or only partially observed.

Here we examine whether EDM-based diagnostics can provide early warning of an impending loss of stability. Using a controlled numerical experiment with known forcing, we test whether changes in forecast skill at multiple horizons, together with local linearization diagnostics derived from a *single observed variable*, anticipate a transition from locally attracting equilibrium behavior to sustained oscillatory dynamics. Throughout, "loss of stability" refers to a transition from a locally attracting equilibrium to a persistent oscillatory regime induced by slow, quasi-static parameter drift.

2 Dynamical System and Experimental Design

2.1 Hastings–Powell tri-trophic model

We consider the Hastings–Powell tri-trophic food chain model describing prey (X), consumer (Y), and top predator (Z):

$$\frac{dX}{dt} = X(1-X) - \frac{c_1 XY}{1+h_1 X}, \tag{1}$$

$$\frac{dY}{dt} = \frac{c_1 XY}{1+h_1 X} - \frac{c_2 YZ}{1+h_2 Y} - m_2 Y, \tag{2}$$

$$\frac{dZ}{dt} = \frac{c_2 YZ}{1+h_2 Y} - m_3 Z. \tag{3}$$

Depending on parameters, this system exhibits either a stable equilibrium or sustained oscillatory dynamics, making it a standard testbed for studying stability loss in nonlinear ecological systems.

2.2 Slow parameter drift

To induce a controlled transition while minimizing sensitivity to initial conditions, we impose a two-phase forcing protocol on the interaction strength $c_2(t)$. An initial burn-in period of duration t_{drift} allows the system to relax toward equilibrium. Following burn-in, $c_2(t)$ is increased linearly:

$$c_2(t) = \begin{cases} c_{2,\text{start}}, & t \le t_{\text{drift}}, \\ c_{2,\text{start}} + \dfrac{t - t_{\text{drift}}}{t_{\max} - t_{\text{drift}}} \left(c_{2,\text{end}} - c_{2,\text{start}}\right), & t > t_{\text{drift}}. \end{cases}$$

The drift rate is chosen to be slow relative to intrinsic system timescales, approximating quasi-static forcing. We assume only the top predator abundance $Z(t)$ is observed.

3 Data Generation and Transition Detection

The system was numerically integrated on a uniform grid ($\Delta t = 1$, $t \in [0, 8000]$).

In the baseline experiment, we set $t_{\text{drift}} = 2000$ and increased c_2 from 0.06 to 0.18. To define a reference transition time independent of EDM, we compute a rolling standard deviation of $Z(t)$ (window $w = 300$) over the full time series and define t^* as the first time the rolling SD exceeds a robust baseline threshold (median + k·MAD, with $k = 3$). This provides a heuristic benchmark for the onset of increased variability and is used only for temporal alignment of diagnostics. In this experiment, the procedure identifies $t^* = 3905$.

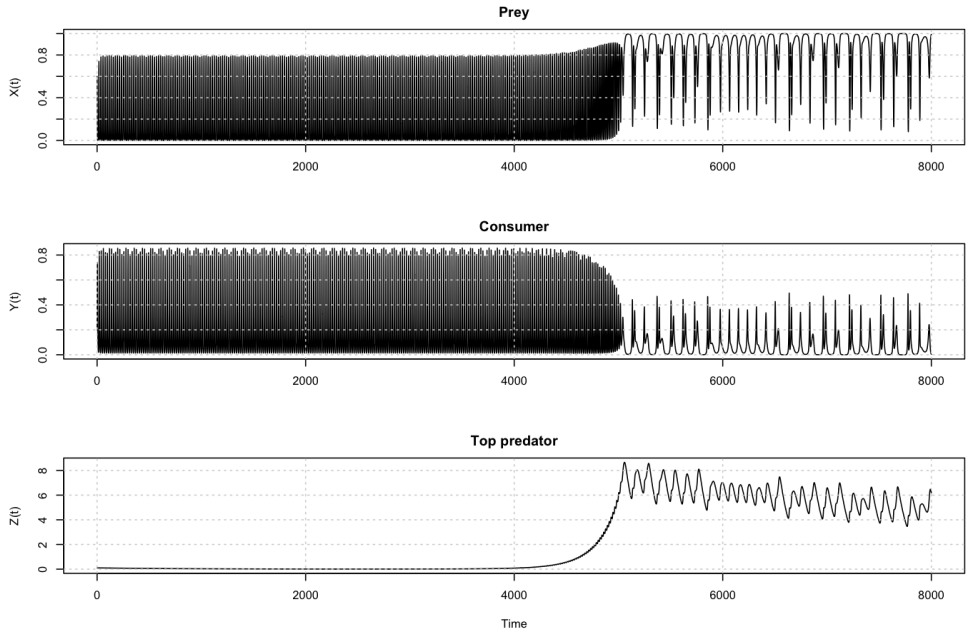

Figure 1: Tri-trophic time series $(X(t), Y(t), Z(t))$ under slow forcing.

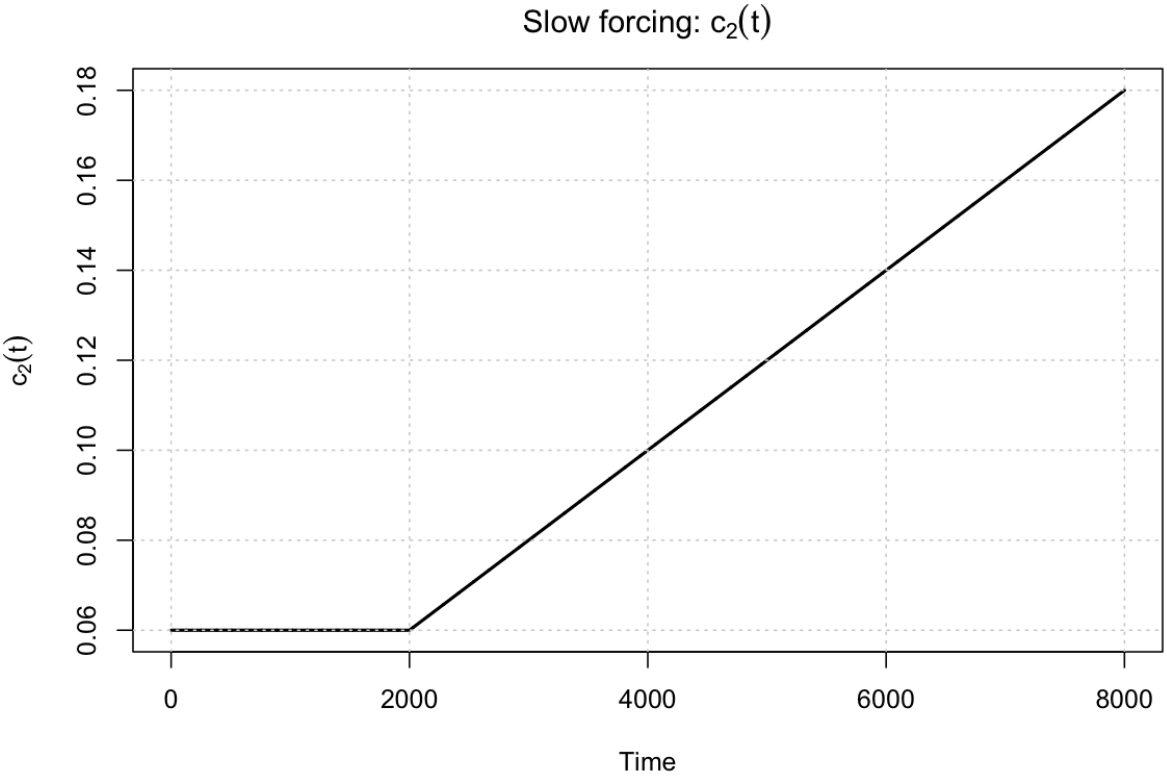

(a) Imposed quasi-static drift in interaction strength $c_2(t)$.

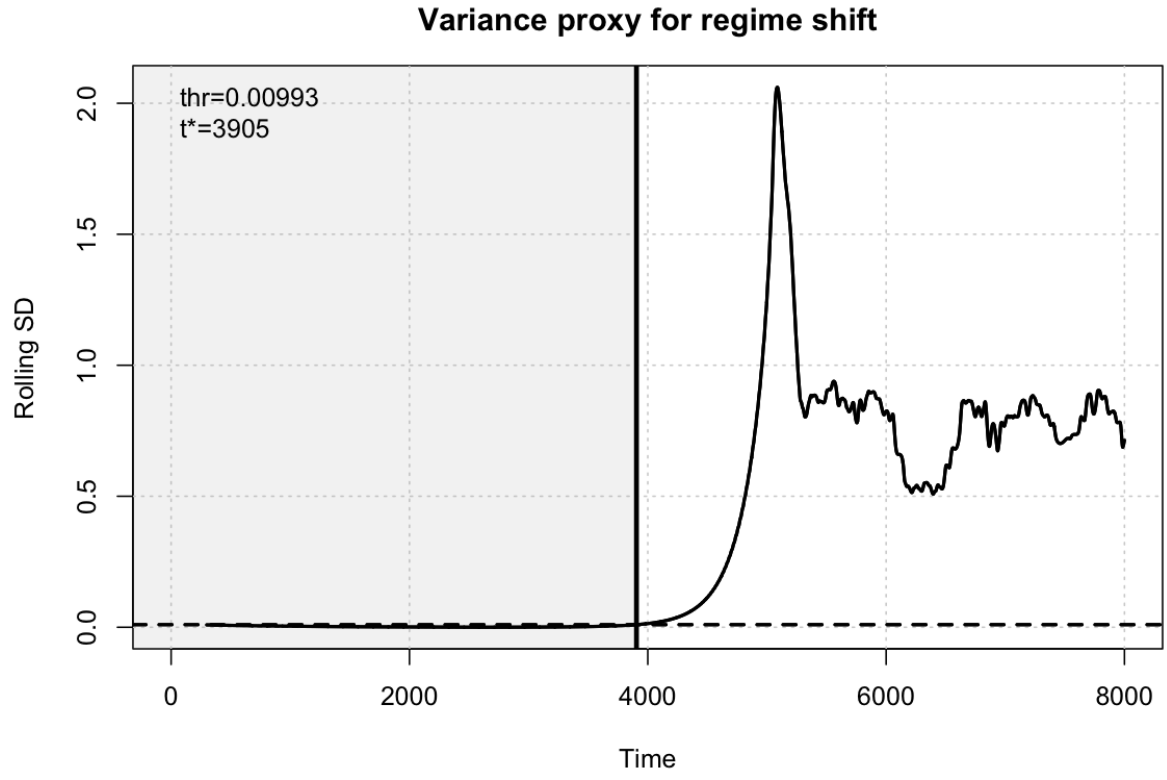

(b) Rolling standard deviation of $Z(t)$ (window $w = 300$) defining the empirical transition time t^*.

Figure 2: Slow forcing and empirical transition detection. Top: forcing protocol $c_2(t)$. Bottom: variance proxy (rolling SD) used to define t^*.

4 Empirical Dynamic Modeling

4.1 Delay-coordinate reconstruction

Using only the observed predator time series $Z(t)$, we reconstruct state via delay coordinates:

$$\mathbf{x}_t = \big(Z_t, Z_{t-\tau}, \ldots, Z_{t-(E-1)\tau}\big),$$

where E is the embedding dimension and τ the delay [2, 3]. Based on false nearest neighbors analysis (Fig. 6), we fix $E = 3$ and $\tau = 1$ throughout. Holding the embedding fixed allows temporal changes in predictability and local linear structure to be attributed to forcing rather than to re-optimizing embedding parameters.

4.2 Sliding-window forecasting

Predictability is quantified using sliding-window Simplex forecasting. Within each window, one-step ($h = 1$) and long-horizon ($h = 10$) forecasts are generated using nearest neighbors in reconstructed space with exponential distance weighting [1]. A Theiler exclusion of 50 time steps prevents temporally adjacent analogs [6]. Forecast skill is evaluated out-of-sample using correlation ρ.

Long-horizon forecasts are more sensitive to weak local expansion rates; thus, earlier degradation at larger horizons is consistent with weakening local stability.

4.3 Local linearization via S-map

S-map estimates a locally weighted linear approximation to the one-step map in reconstructed space:

$$Z_{t+1} \approx a(t) + \boldsymbol{\beta}(t)^\top \mathbf{x}_t,$$

with coefficients obtained via locally weighted least squares [2, 4]. We track the coefficient associated with the contemporaneous coordinate Z_t,

$$b(t) := \frac{\partial \hat{Z}_{t+1}}{\partial Z_t},$$

as a scalar proxy for local contraction or expansion along the observed dimension. Values approaching $|b(t)| \approx 1$ indicate weakened contraction, and increasing dispersion of $b(t)$ reflects increasing heterogeneity in local linear behavior.

4.4 State dependence

To quantify state dependence, we sweep the localization parameter θ in each window, identify the optimal $\theta^*(t)$ maximizing one-step forecast skill, and compute the predictive gain

$$\Delta\rho(t) = \rho\big(t, \theta^*(t)\big) - \rho(t, 0).$$

Positive $\Delta\rho(t)$ indicates that state-dependent local structure improves prediction relative to a global linear approximation [4].

Interpretation caveat

All diagnostics are derived from a single scalar observable and a low-dimensional delay reconstruction. They should be interpreted as empirical indicators of changing local geometry and predictability, not as direct mechanistic estimates of the full system Jacobian.

5 Results

5.1 Forecast skill degradation

Sliding-window forecast skill (Fig. 3) changes markedly through the destabilization interval surrounding the empirical transition benchmark t^*. In particular, long-horizon forecasts ($h = 10$) exhibit stronger degradation during the period of rapidly increasing variability, consistent with growing sensitivity to initial conditions. After oscillations emerge and the system settles onto a coherent attractor, forecast skill partially recovers.

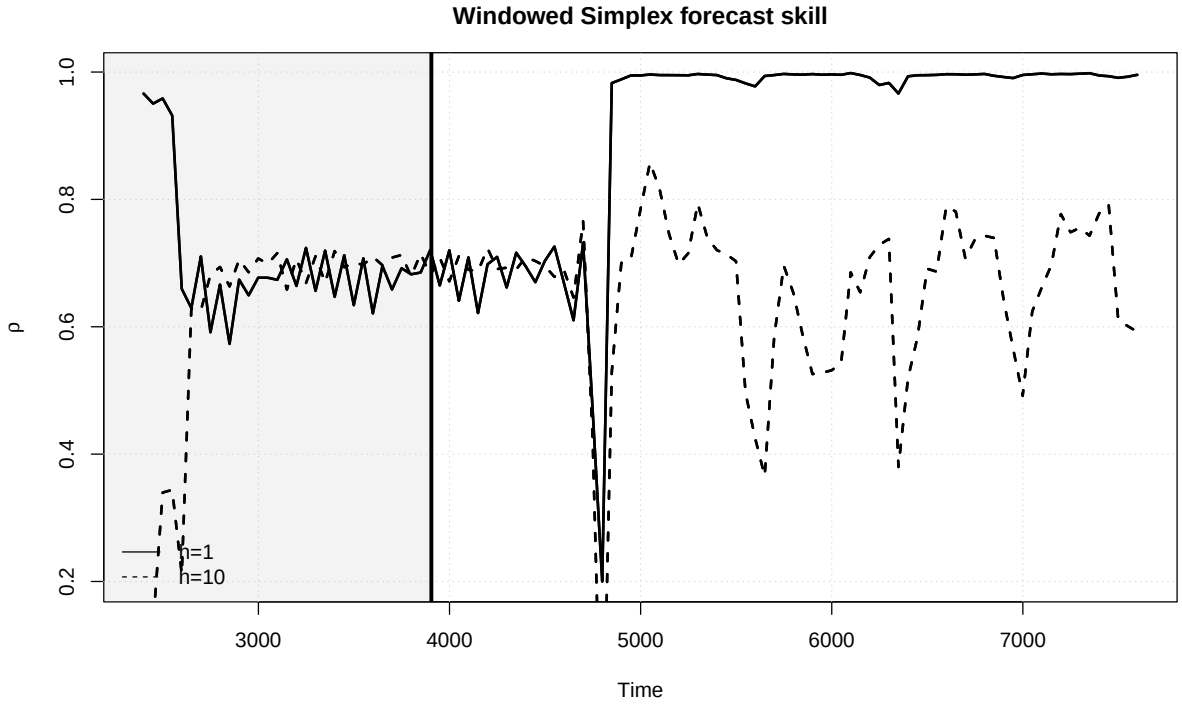

Figure 3: Sliding-window forecast correlation for one-step ($h = 1$) and long-horizon ($h = 10$) predictions. Vertical line indicates the empirical transition time t^*.

5.2 Local stability diagnostics

Median S-map slopes and within-window dispersion (Fig. 4) show signatures consistent with weakening contraction prior to the transition. Median coefficients approach $|b| \approx 1$ and slope dispersion increases, indicating greater heterogeneity in local linearization of the reconstructed map.

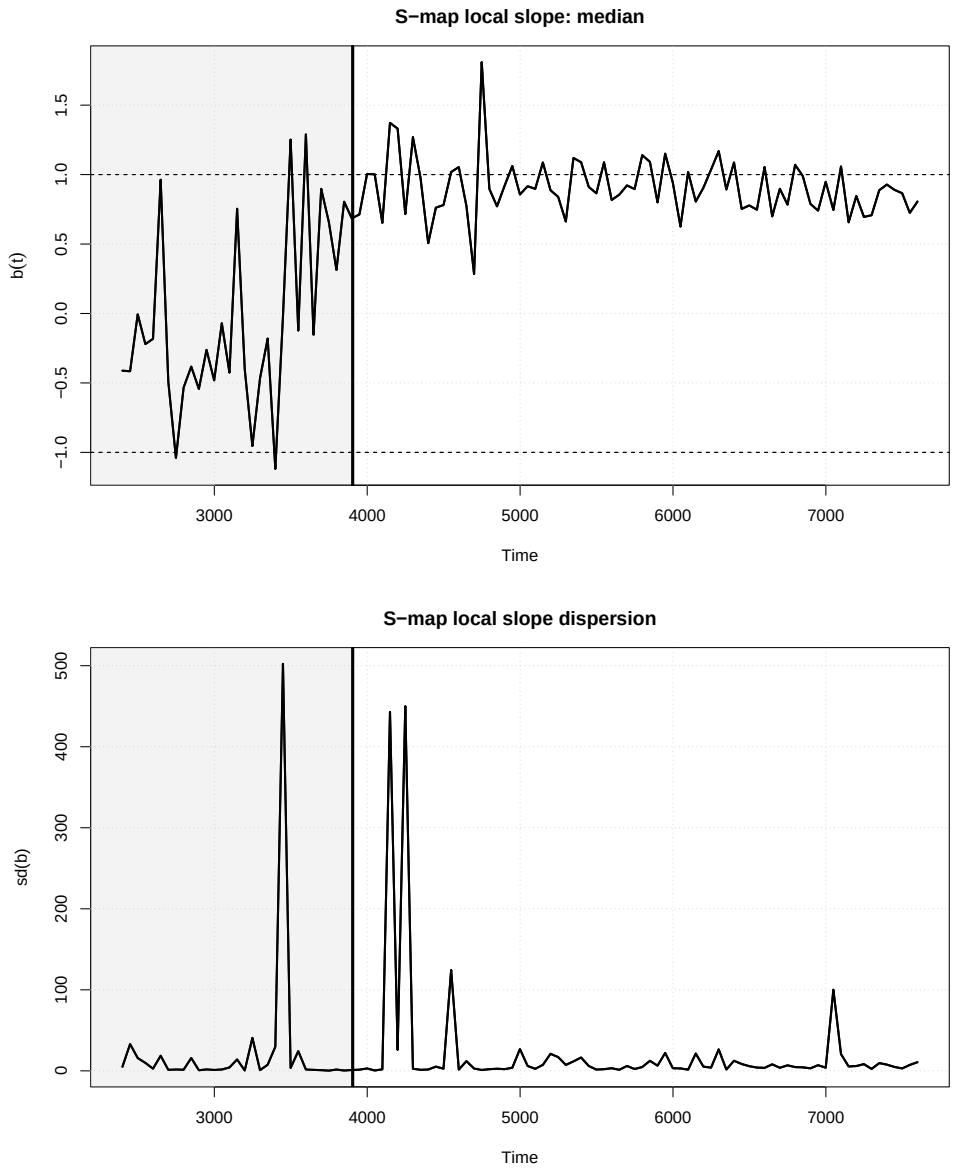

Figure 4: Sliding-window local linearization diagnostics from S-map. Top: median slope $b(t) = \partial \hat{Z}_{t+1}/\partial Z_t$. Bottom: within-window standard deviation of $b(t)$.

5.3 State dependence

State-dependence diagnostics show weak and parameter-sensitive structure across the transition (Fig. 5). In this controlled, noise-free setting, global linear S-map models often achieve predictive skill comparable to localized fits ($\theta^* \approx 0$), limiting the strength of state-dependence signals. This behavior is consistent with smoothly forced dynamics in which nonlinear geometry evolves gradually rather than abruptly.

After oscillations emerge, both measures decline as the dynamics settle into a more homogeneous oscillatory attractor.

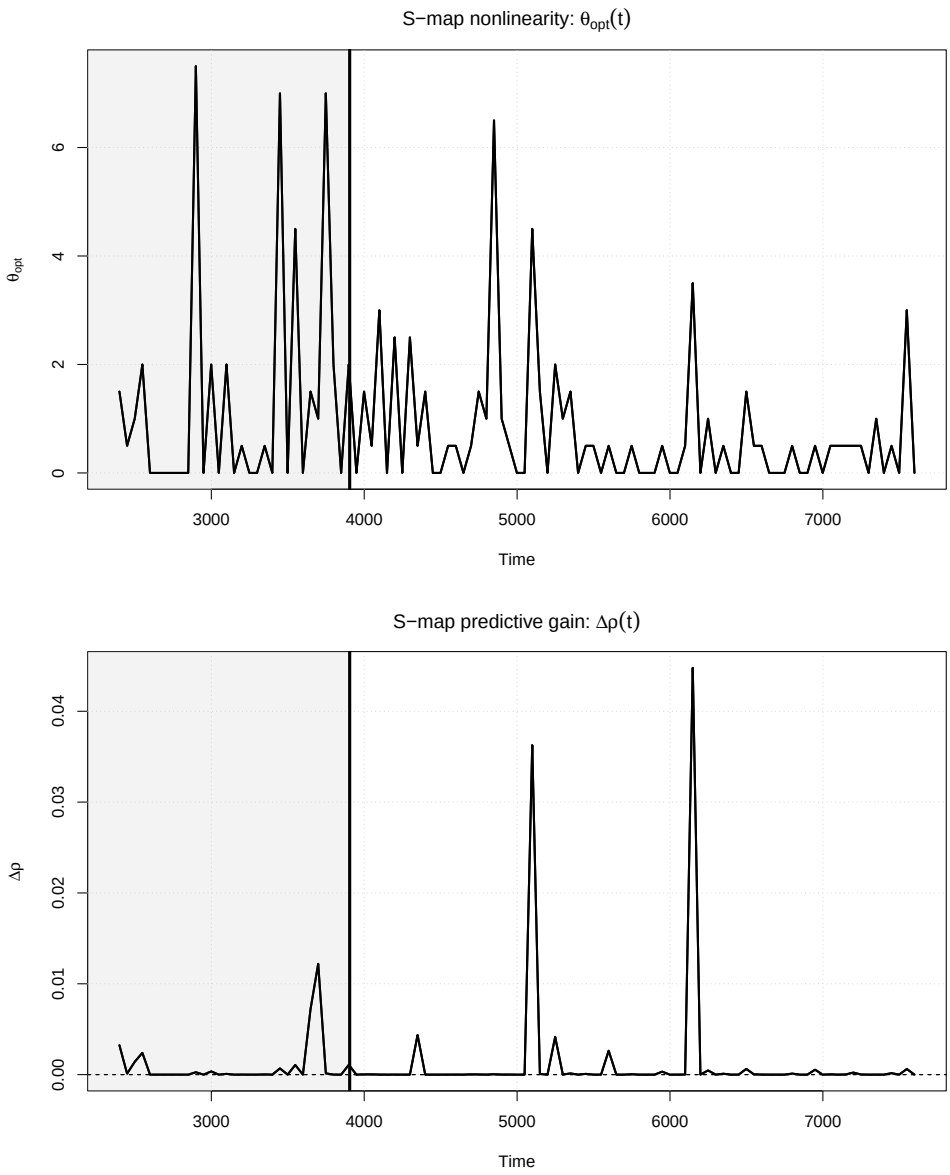

Figure 5: Sliding-window S-map state-dependence diagnostics. Top: optimal localization parameter $\theta^*(t)$. Bottom: predictive gain $\Delta\rho(t)$ relative to a global linear model ($\theta = 0$).

5.4 Sensitivity analysis

To assess robustness, we repeated the windowed EDM diagnostics over multiple analysis window sizes ($W \in \{600, 800, 1000\}$) and transition-detection windows ($w \in \{200, 300\}$). Across this grid, the qualitative early-warning patterns persisted, while trend magnitudes varied with windowing choices, motivating sensitivity reporting rather than single-run claims. A full summary of sensitivity results is provided in the accompanying repository (`results/sensitivity_summary.csv`).

6 Embedding Dimension Validation

False nearest neighbors provides an embedding diagnostic independent of EDM forecast-skill tuning. Applied to the post-drift predator dynamics $Z(t)$, the fraction of false neighbors drops sharply between $E = 2$ and $E = 3$ and remains near zero thereafter, indicating that $E = 3$ is sufficient to unfold the attractor.

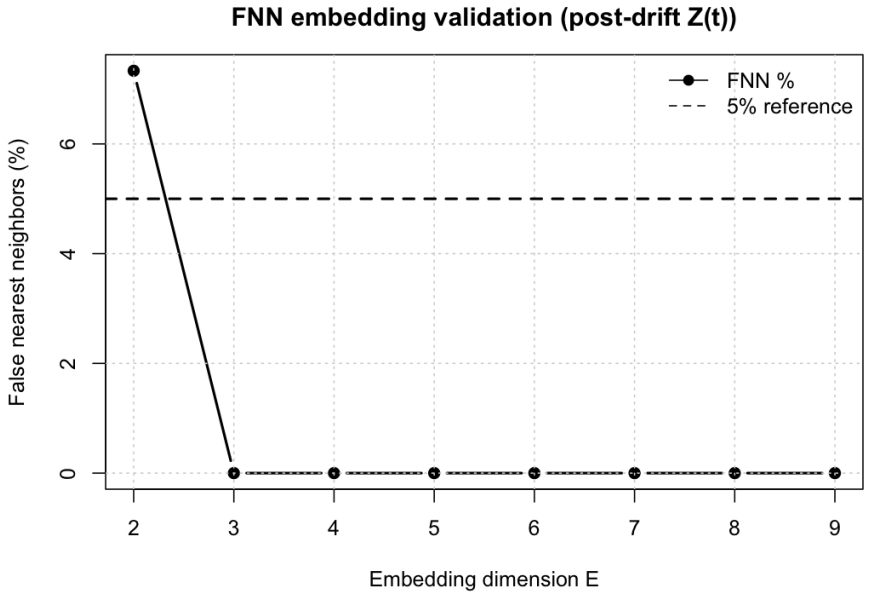

Figure 6: False nearest neighbors (FNN) analysis on post-drift predator dynamics $Z(t)$. A sharp decrease from $E = 2$ to $E = 3$ with near-zero values at higher E supports the use of $E = 3$ in delay-coordinate reconstruction.

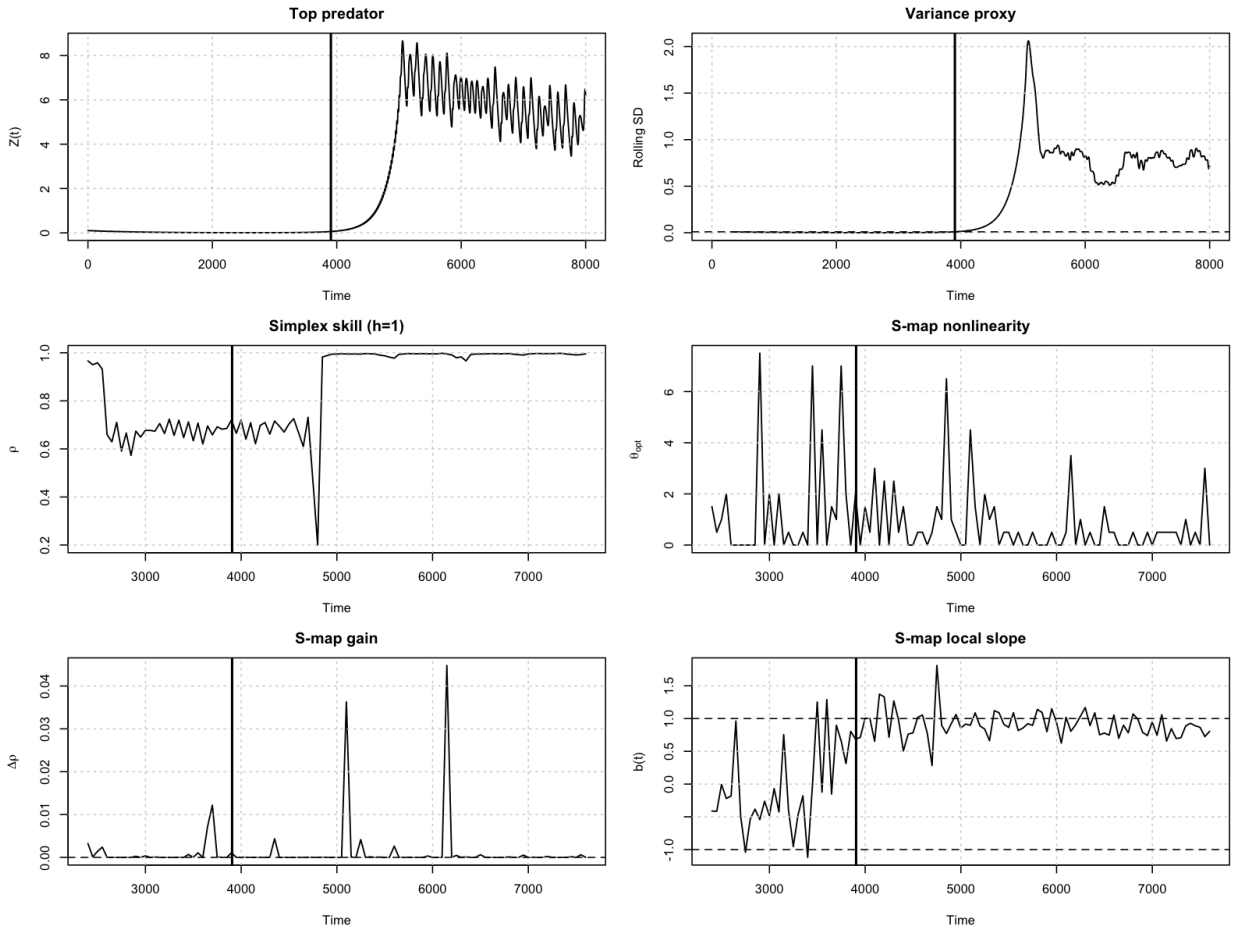

Figure 7: Summary of early-warning diagnostics aligned to the empirical transition time t^*. This panel consolidates predictability degradation (Simplex), local linearization behavior (S-map slopes), and state dependence (S-map θ^* and $\Delta\rho$) into a single view suitable for rapid assessment.

7 Discussion

Across three complementary diagnostics—forecast skill degradation, weakening local contraction (via S-map slope behavior), and increasing state dependence—we observe coordinated early warning signatures preceding the loss of equilibrium stability. Unlike moment-based indicators, EDM diagnostics interrogate reconstructed dynamics directly and quantify changes in predictability and local geometric structure.

A key interpretation is temporal: the strongest signals appear during destabilization. After the transition, predictability partially recovers as the system approaches a coherent oscillatory attractor. Thus, "predictability" is not synonymous with "equilibrium stability": an oscillatory attractor can be geometrically regular and hence predictable, even though the original equilibrium has lost stability.

These results are empirical and data-driven. Their utility depends on sampling density and on how well the reconstructed state space is populated; performance may degrade under strong observational noise, sparse sampling, or severe nonstationarity.

Fig. 7 summarizes the coordinated signal across diagnostics.

We emphasize that state-dependence diagnostics were weaker than predictability and local linearization indicators in this experiment. This reflects the highly deterministic and smoothly forced nature of the system, where global models already achieve near-optimal prediction. In more weakly observed or noisy systems, state-dependent gains may play a larger role.

Importantly, these diagnostics require no explicit model specification and operate directly on observed time series, making them applicable to a broad class of complex systems beyond ecology.

8 Conclusion

EDM-based predictability and local linearization diagnostics provide empirically grounded early warning signals of stability loss from a single observed variable. Declines in long-horizon forecast skill, convergence of local coefficients toward $|b| \approx 1$ with increasing heterogeneity, and elevated state dependence consistently precede the empirical onset of oscillations, highlighting the potential of EDM for monitoring nonlinear, forced systems. These results suggest that EDM-based diagnostics may be useful as model-agnostic monitoring tools in systems where governing equations are unknown, partially observed, or subject to slow external forcing.

References

[1] G. Sugihara and R. M. May. Nonlinear forecasting as a way of distinguishing chaos from measurement error in time series. *Nature*, 344:734–741, 1990.

[2] G. Sugihara. Nonlinear forecasting for the classification of natural time series. *Philosophical Transactions of the Royal Society A*, 348:477–495, 1994.

[3] G. Sugihara et al. Detecting causality in complex ecosystems. *Science*, 338:496–500, 2012.

[4] H. Ye, R. J. Beamish, S. M. Glaser, S. C. Hsieh, L. J. C. Hsu, G. Sugihara, and E. M. Sugihara. Equation-free mechanistic ecosystem forecasting using empirical dynamic modeling. *Proceedings of the National Academy of Sciences*, 112(13):E1569–E1576, 2015. doi:10.1073/pnas.1417063112.

[5] V. Dakos et al. Methods for detecting early warnings of critical transitions. *PLoS ONE*, 7:e41010, 2012.

[6] J. Theiler. Spurious dimension from correlation algorithms applied to limited time-series data. *Physical Review A*, 34(3):2427–2432, 1986.